Analyst

ROYAL SOCIETY OF CHEMISTRY

PAPER

View Article Online
View Journal | View Issue

Cite this: *Analyst*, 2024, **149**, 386

A promising electrochemical sensor based on PVP-induced shape control of a hydrothermally synthesized layered structured vanadium disulfide for the sensitive detection of a sulfamethoxazole antibiotic†

Mingjiao Shi,[a,b] Peizheng Shi,[b] Xinxin Yang,[a] Ningbin Zhao,[b] Mengfan Wu,[b] Jing Li,[c] Chen Ye,[b,d,e] He Li,[b,d,e] Nan Jiang,[b,d,e] Xiufen Li,[f] Guosong Lai,[g] Wan-Feng Xie,[h] Li Fu,[i] Gang Wang,[j] Yangguang Zhu,*[b,f] Hsu-Sheng Tsai*[c,k] and Cheng-Te Lin*[b,d,e]

The presence of sulfamethoxazole (SMX) in natural waters has become a significant concern recently because of its detrimental effects on human health and the ecological environment. To address this issue, it is of utmost urgency to develop a reliable method that can determine SMX at ultra-low levels. In our research, we utilized PVP-induced shape control of a hydrothermal synthesis method to fabricate layer-like structured VS_2, and employed it as an electrode modification material to prepare an electrochemical sensor for the sensitive determination of SMX. Thus, our prepared VS_2 electrodes exhibited a linear range of 0.06–10.0 μM and a limit of detection (LOD) as low as 47.0 nM (S/N = 3) towards SMX detection. Additionally, the electrochemical sensor presented good agreement with the HPLC method, and afforded perfect recovery results (97.4–106.8%) in the practical analysis. The results validated the detection accuracy of VS_2 electrodes, and demonstrated their successful applicability toward the sensitive determination of SMX in natural waters. In conclusion, this research provides a promising approach for the development of electrochemical sensors based on VS_2 composite materials.

Received 6th August 2023,
Accepted 6th November 2023

DOI: 10.1039/d3an01355c

rsc.li/analyst

Introduction

Sulfamethoxazole (SMX) is a synthetic antibiotic with a broad antibacterial spectrum of activity.[1,2] It is particularly, effective against *Staphylococcus aureus* and *Escherichia coli*. It finds widespread application in the medical, agricultural, and animal husbandry industries, making it one of the most utilized sulfonamide medications.[3] However, according to the World Health Organization's International Agency for Research on Cancer (IARC), sulfamethoxazole has been classified as a Group 3 carcinogen in their 2017 list of carcinogens.[4] The reason behind this classification lies in the fact that sulfamethoxazole is a large molecular organic compound that exhibits limited degradation capabilities. Living organisms in a

[a]*School of Materials Science and Engineering, Shanghai University, Shanghai, 200072, P.R. China*
[b]*Qianwan Institute, Ningbo Institute of Materials Technology and Engineering (NIMTE), Chinese Academy of Sciences, Ningbo 315201, China*
[c]*School of Physics, Harbin Institute of Technology, 150001 Harbin, China. E-mail: hstsai@hit.edu.cn*
[d]*Center of Materials Science and Optoelectronics Engineering, University of Chinese Academy of Sciences, Beijing 100049, China*
[e]*Key Laboratory of Marine Materials and Related Technologies, Zhejiang Key Laboratory of Marine Materials and Protective Technologies, Ningbo Institute of Materials Technology and Engineering (NIMTE), Chinese Academy of Sciences, Ningbo 315201, China. E-mail: linzhengde@nimte.ac.cn*
[f]*Laboratory of Environmental Biotechnology, School of Environmental and Civil Engineering, Jiangnan University, Wuxi, 214122, China. E-mail: zhuyangguang@nimte.ac.cn*
[g]*Hubei Key Laboratory of Pollutant Analysis & Reuse Technology, College of Chemistry and Chemical Engineering, Hubei Normal University, Huangshi, 435002, China*
[h]*College of Electronics and Information, University-Industry Joint Center for Ocean Observation and Broadband Communication, Qingdao University, Qingdao, 266071, China*
[i]*College of Materials and Environmental Engineering, Hangzhou Dianzi University, Hangzhou 310018, China*
[j]*Department of Microelectronic Science and Engineering, School of Physical Science and Technology, Ningbo University, Ningbo, 315211, China*
[k]*Laboratory for Space Environment and Physical Sciences, Harbin Institute of Technology, 150001 Harbin, China*

† Electronic supplementary information (ESI) available. See DOI: https://doi.org/10.1039/d3an01355c

sulfamethoxazole-contaminated environment might experience compromised growth and reproductive capabilities.[5] It is true that these antibiotics can enter the human body through the enrichment effect of the food chain, thereby posing a risk to human health. Therefore, ensuring the sensitive detection of sulfamethoxazole is of utmost importance.

Presently, the detection methods for sulfamethoxazole mainly consist of spectrophotometry, high-performance liquid chromatography (HPLC),[6,7] enzyme-linked immunosorbent assay (ELISA),[8] capillary electrophoresis,[9,10] and several other techniques. Nevertheless, the application of traditional detection methods in antibiotic detection technology is significantly impeded by the need for costly equipment, intricate sample preparation, and time-intensive detection procedures.[11] On the other hand, electrochemical detection techniques have gained significant attention due to their inherent advantages of being fast, straightforward, portable, and cost-effective.[12] The careful selection of appropriate electrode modification materials is a critical step in the electrochemical detection process.

In the past few years, the field of inorganic nanomaterials has witnessed a remarkable surge in interest, largely attributed to their exceptional physicochemical properties.[13] In particular, transition metal dichalcogenides (TMDCs) like MoS_2, WS_2, and VS_2 have gained considerable attention ascribed to their distinct morphology and graphene-like properties.[14,15] These materials demonstrate excellent chemical, physical, optical, mechanical, magnetic, and electrical characteristics.[16] Layered transition metal dichalcogenide (TMD) crystals are composed of interconnected layers connected by strong in-plane covalent bonds.[17] Meanwhile, the S–M–S interlayer structure, which consists of sulfur molecules (S) and transition metals (M), is held together by comparatively weaker out-of-plane van der Waals forces.[18,19] The distinctive structural characteristics of TMD crystals contribute to their extensive range of physicochemical properties, notably a significant specific surface area and impressive conductivity.[20] These attributes have facilitated their exceptional performance in various fields, including electrocatalysis, lithium-ion batteries, optoelectronic devices, and energy storage.[21] Consequently, TMDs have become a focal point of intense research and development in the past few decades.[22] Among different TMDs, vanadium disulfide (VS_2) stands out as an exemplary material. Recent advancements in first-principles theoretical calculations and experimental research have demonstrated the remarkable properties of two-dimensional layered VS_2, which include excellent conductivity, a high aspect ratio, ultrathin edges, and favorable mechanical characteristics.[23,24] Consequently, VS_2 fulfills the essential criteria for an effective electrochemical sensor. Karthik *et al.* developed a promising non-enzymatic electrochemical sensor for detecting hydrogen peroxide based on a simple sonochemical synthesis of novel grass-like vanadium disulfide.[16] Vilian *et al.* employed a facile hydrothermal method to synthesize electrodes comprising gold nanoparticles decorating VS_2-reduced graphene oxide sheets, achieving a calibration dynamic range of 10–340 nM and a limit of detection (LOD) as low as 0.44 nM towards sulfadiazine detection.[25] Therefore, the incorporation of two-dimensional VS_2 nanocrystals holds great potential in the manufacturing of electrochemical sensors.[26] However, to propose a promising VS_2-based electrochemical platform, comprehensive studies focusing on the structural regulation and electrochemical optimization of VS_2 are still deficient and necessary.

In this work, we utilized the PVP-induced shape control of a hydrothermal synthesis method to fabricate layered structured VS_2, and employed it for the first time as an electrode modification material to prepare an electrochemical sensor for sensitive SMX detection in natural waters. The features and properties of the synthesized material were studied using various characterization methods. Various electrochemical techniques were further applied for evaluating the detection performance of the electrochemical sensor. In particular, the differential pulse voltammetry (DPV) analysis demonstrated that the sensor exhibited high sensitivity and a wide linear range, indicating its substantial potential for environmental water analysis applications.

Experimental

Chemicals

Phosphate buffer solution (10× PBS, containing 1.37 M NaCl, 26.8 mM KCl, 81.0 mM Na_2HPO_4, and 17.6 mM KH_2PO_4) was purchased from Sangon Biotech (Shanghai) Co., Ltd (Shanghai, China). H_2SO_4, potassium ferricyanide ($K_3[Fe(CN)_6]$), potassium hexacyanoferrate(II) ($K_4[Fe(CN)_6]$), and ammonium hydroxide ($NH_3{\cdot}H_2O$) were purchased from Sinopharm Chemical Reagent Co., Ltd (Shanghai, China). Polyvinylpyrrolidone (PVP), ammonium metavanadate (NH_4VO_3), and thioacetamide (TAA) were purchased from Sigma Aldrich (Shanghai) Trading Co., Ltd (Shanghai, China). Sulfamethoxazole, trimethoprim (TMP), furazolidone (FRZ), erythromycin (ERY), chloramphenicol (CPL), and glucose (Glu) were purchased from Shanghai Aladdin Bio-Chem Technology Co., Ltd (Shanghai, China). All chemical reagents used in our experiments were of analytical grade and used without further purification. Milli-Q deionized water was used throughout our tests.

Fabrication of VS_2 electrodes

The preparation method of VS_2 nanosheets is presented as follows. 1.0 g PVP was dissolved in a mixture comprising 30 mL of deionized water and 2 mL of $NH_3{\cdot}H_2O$. Then 0.234 g of NH_4VO_3 and 1.5 g of TAA were added into the mixture sequentially. After being subjected to magnetic stirring at room temperature for 1 hour, the mixture was transferred into a Teflon-lined stainless-steel autoclave with a volume of 50 mL, and heated at 180 °C for 20 h. The product was collected by employing centrifugation and washed repeatedly with anhydrous ethanol. Subsequently, the washed product was vacuum-dried at 60 °C for 24 h. Finally, VS_2 nanosheets were obtained by annealing for 2 h under a N_2 atmosphere at 300 °C at a rate of 2 °C min^{-1}.[27] Finally, a 1 mg mL^{-1} dispersion of tVS_2

nanosheets was prepared and preserved for the following experiments.

Before the electrode modification, glassy carbon electrodes (GCEs) with a 3 mm diameter were first polished using a 0.05 μm alumina slurry. Subsequently, the electrodes were subjected to ultrasonication in deionized water and ethanol to ensure thorough cleaning. Following the thorough cleaning, GCEs were scanned *via* repetitive potential range scanning from −1 to 1 V in 0.5 M sulfuric acid at a scan rate of 100 mV s^{-1} to activate the electrodes. Finally, a 8 μL droplet of aqueous VS_2 dispersion was drop-coated on GCE and dried at 60 °C for 10 min to obtain VS_2 electrodes.

Analytical tests

For the experiment, 1× PBS obtained after 10 times dilution of 10× PBS was used as the electrolyte. The VS_2 electrodes were used as working electrodes, while a saturated calomel electrode (SCE) and a Pt electrode were employed as the reference electrode and counter electrode, respectively. Cyclic voltammetry (CV), DPV and electrochemical impedance spectroscopy (EIS) tests were performed to analyse the voltammetric responses of various modified electrodes. CV curves were conducted from −0.2 to 0.6 V in five cycles at a scan rate of 0.2 V s^{-1}, while DPV tests were performed from 0.7 to 1.1 V with the parameters as: pulse period of 0.5 s, step potential of 0.004 V and amplitude of 0.005 V. EIS was performed in the range of 0.1–100 kHz with a 10 mV amplitude of AC voltage. All our electrochemical tests were conducted using a CHI660e electrochemical workstation (Shanghai Chenhua Co., LTD, China). The zeta potential of the VS_2 dispersion and SMX aqueous solution were determined using a dynamic light scattering-zeta instrument (Zeta potential, Zetasizer Ultra, UK). HPLC (e2695-2998, Waters, Ireland) was applied for the SMX determination in real samples.

Characterization

Field emission scanning electron microscopy (FE-SEM QUANTA 250 FEG, FEI, Hills-boro, OR, USA), energy dispersive spectroscopy (EDS), and transmission electron microscopy (TEM, JEM-2100F, JEOL, Japan) were employed to observe the morphology of the modified material. Raman spectroscopy (Renishaw inVia Reflex, Renishaw plc, Wotton-under-Edge, London, UK) with a laser wavelength of 532 nm and X-ray diffraction (XRD, D8 Advance, Germany) with Cu Kα radiation (λ: 1.54 Å) were applied for the elemental analysis and crystalline structure analysis of the synthesized material. X-ray photoelectron spectroscopy (XPS, Axis SUPRA+, Shimadzu, Japan) was used to indicate the surface compositions and chemical states.

Results and discussion

PVP-induced shape control of the preparation of layer-by-layer stacked VS_2 nanosheets

The schematic diagram shown in Fig. 1 depicts the preparation process of layer-by-layer stacked VS_2 nanosheets by a PVP-induced shape control method. After thoroughly combining

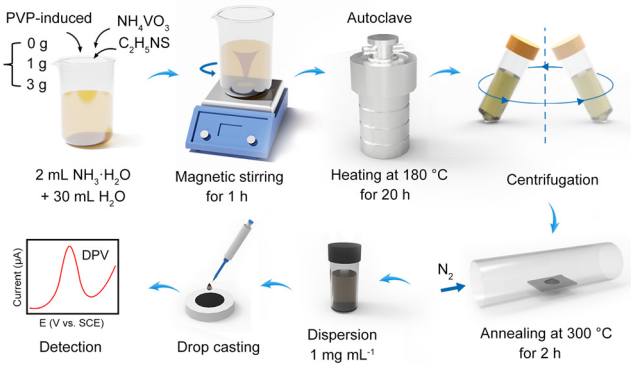

Fig. 1 Schematic diagram of the preparation process and SMX detection of the VS_2 electrode.

0.234 g of NH_4VO_3 with 1.500 g of TAA, the mixture was dissolved in an alkaline solution by adding 0, 1.000, and 3.000 g PVP, respectively. The resulting mixture underwent a hydrothermal process, where it was kept at 180 °C for 20 h. Following that, annealing was carried out at 300 °C for 2 h to synthesize layer-by-layer stacked VS_2 nanosheets, named VS_2 – A, VS_2 – B and VS_2 – C. The morphology evolution of VS_2 nanosheets induced by PVP is illustrated in Fig. 2a. The morphology of VS_2 – A prepared without PVP showed an elongated and hexagonal structure, as seen in Fig. 2b. Interestingly, the morphology of VS_2 transformed from a hexagonal to a circular

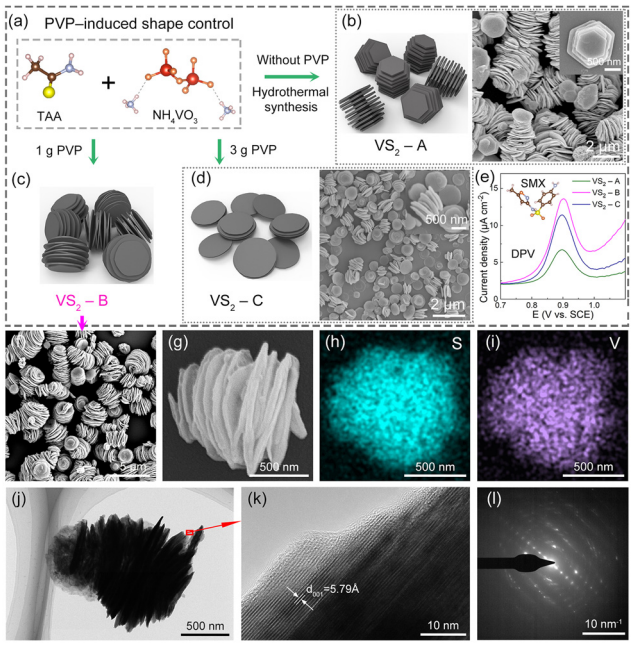

Fig. 2 (a) A schematic illustration of layer-by-layer stacked VS_2 nanosheets prepared by the PVP-induced shape control method. (b–d) The scheme and SEM image of VS_2 – A, VS_2 – B and VS_2 – C. (e) DPV curves of the VS_2 – A, VS_2 – B and VS_2 – C electrodes with 10 μM SMX. SEM images of VS_2 – B at (f) low and (g) high magnification. EDS elemental mapping of (h) V and (i) S. (j) TEM image, (k) HRTEM image and (l) the corresponding SAED patterns of VS_2 nanosheets.

structure and its stacked layers were found to be exfoliated into a structure like an accordion with the addition of PVP, as presented in Fig. 2c. PVP, as an anionic surfactant, possesses hydroxyl groups at the ends of its molecules and can be adsorbed onto VS_2 layers through electrostatic interactions.[21] With the aid of PVP, the stacked layers of VS_2 were inclined to be exfoliated through sonication in the dispersion. By increasing the amount of PVP to 3.000 g, stacked VS_2 nanosheets were further exfoliated into fewer layers, as shown in Fig. 2d. The purity of the prepared VS_2 samples was confirmed by TEM elemental mapping and elemental composition, as presented in Fig. S1 and Table S1.†

To determine the optimal structure of VS_2 induced by PVP, the DPV curvesof VS_2 – A, VS_2 – B and VS2 – C electrodes were constructed for 10 μM SMX, as shown in Fig. 2e. The results demonstrated that the VS_2 – B electrodes exhibited the best electrochemical response toward SMX, which was chosen as the optimized VS_2 nanosheet for the following experiments. Compared to the stacked layers of VS_2 – A, the VS_2 – B layers tended to be exfoliated by the induced regulation of PVP. A higher specific surface area of VS_2 – B electrodes enhanced the adsorption capability of SMX, presentinga better electrochemical response.[28] When regulated with excess PVP, the VS_2 – C electrodes showed a dispersed structure with fewer layers, decreasing its adsorption capability towards SMX. Thus, VS_2 – B indicates the priority towards SMX detection.

Characterization of layer-by-layer stacked VS_2 nanosheets

The SEM images in Fig. 2f and g depict the morphology of VS_2. VS_2 was composed of vertically stacked nanosheets, exhibiting a diameter and thickness of up to 500–1000 nm and 20–30 nm approximately. Elemental analysis using an energy-dispersive spectrometer (EDS) confirmed the presence and uniform distribution of V and S elements, as shown in Fig. 2h and i. TEM and high-resolution TEM (HRTEM) images revealed the crystal structure of VS_2, as presented in Fig. 2j and k. TEM images revealed that the VS_2 nanosheets were stacked in the [001] direction, with an interlayer spacing of approximately 5.79 Å.[21] This value closely matches the normal interplanar spacing (5.76 Å) of the original VS_2 (001) plane.[29] Electron diffraction was employed to demonstrate the polycrystalline nature of the synthesized sample, as indicated in Fig. 2l.

Fig. 3a presents the crystal structure (the unit cell and molecules) of VS_2, referenced from the PDF card number 89-1640. From the observation in Fig. 3a, each layer of vanadium disulfide consists of a vanadium layer sandwiched between two sulfur layers, and the sandwiched structures are connected by van der Waals forces.[18]

From the XRD patterns (Fig. 3b), all the observed diffraction peaks in the graph can be assigned to VS_2 (JCPDS#89-1640), with lattice constants of $a = b = 3.22$ Å and $c = 5.76$ Å. These findings provide further confirmation of the successful formation of VS_2 nanosheets with regular interlayer spacing. The chemical structure of the synthesized VS_2 was investigated using Raman spectroscopy, as shown in Fig. 3c. It displayed characteristic vibration bands at nearly 281 and 405 cm^{-1},

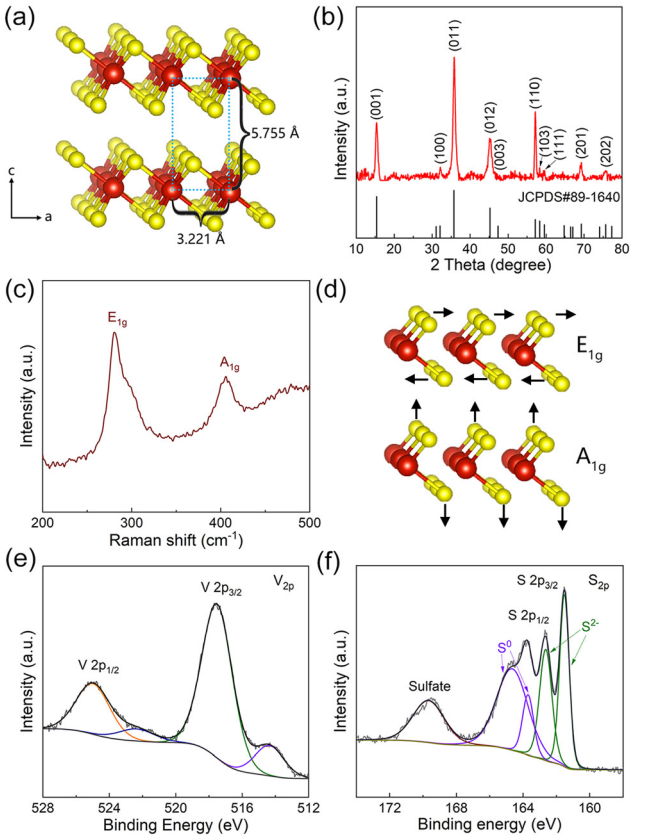

Fig. 3 (a) A schematic representation of the crystal structure of VS_2 nanosheets. (b) XRD patterns, and (c) Raman spectra of VS_2 nanosheets. (d) Vibration bonds of VS_2 nanosheets. High-resolution XPS spectra at (e) V_{2p} and (f) S_{2p} regions of VS_2 nanosheets.

corresponding to E_{1g} and A_{1g} modes, respectively.[30] These modes represent the in-plane vibration (E_{1g}) and out-of-plane vibration (A_{1g}) of the S–V–S bonds,[31] as depicted in Fig. 3d. In fact, the Raman signals of VS_2 demonstrate an analogy to other transition metal sulfides within the vanadium group.[32,33]

In Fig. 3e, the high-resolution XPS spectrum of V 2p unveiled two prominent peaks centered at approximately 525.0 and 517.5 eV. These peaks are assigned to V $2p_{1/2}$ and V $2p_{3/2}$, respectively, affirming the existence of the V^{4+} oxidation state.[34] Additionally, the XPS spectrum also exhibits two smaller peaks located at approximately 522.2 and 514.2 eV. These minor peaks suggested the presence of a small quantity of V^{2+} ions, which can be attributed to the reducing properties of organic amines and the strong reducing nature of hydrogen sulfide generated from the decomposition of thioacetamide in the preparation.[35] The XPS spectrum of S 2p shown in Fig. 3f showed distinct peaks at around 162.7 and 161.5 eV, corresponding to S $2p^{1/2}$ and S $2p^{3/2}$ of S^{2-} species.[36] Peaks located at around 163.7 and 164.5 eV are attributed to the S^0 species, while the peak at around 169.6 eV can be assigned to the sulfate species.[37] These results indicated that slight oxidation and contamination with elemental sulfur and sulfates occurred in the VS_2 sample due to its exposure to air.

Performance optimization of VS_2/GCE electrodes toward SMX detection

To investigate the electrochemical performance of VS_2 towards SMX, the electron transfer ability of VS_2 electrodes needs to be understood. The oxidation peak with potential 0.90 V was designated as the characteristic peak for SMX electrochemical analysis. To assess the interfacial charge transfer ability, EIS was performed on GCE and VS_2 electrodes in 10 mM $[Fe(CN)_6]^{3-/4-}$ (Fig. 4a). Through the model simulation according to its Nyquist curves, the equivalent circuit model of VS_2 electrodes is equivalent to $R_s(Q_{dl}(R_{ct}(Q_c(R_c{\cdot}Z_W))))$. In particular, R_{ct} denotes the interfacial electron transfer resistance and determines the electron transfer ability on various electrodes.[38] The R_{ct} values of VS_2 electrodes and GCE were 567.2 and 5079.0 Ω, respectively. The R_{ct} value of GCE was higher than that for VS_2 electrodes, demonstrating that VS_2 enhances the charge transfer ability of electrodes. The fitted values of various parameters in the model are presented in Table S2.†

To further enhance the detection performance of VS_2 electrodes, analytical parameters such as the modified mass of VS_2 on the electrode, scan rates, and electrolyte pH were treated in optimization. To determine the appropriate mass of VS_2 during electrode preparation, the DPV curves of VS_2 electrodes modified with various masses of VS_2 as 2, 4, 6, 8, 10 and 12 μg were constructed for PBS containing 10 μM SMX. As shown in Fig. 4b, 8 μg of VS_2 was selected for further experiments. To evaluate the electrochemical behaviors on the VS_2 electrode surface, CV responses were obtained in 10 mM $[Fe(CN)_6]^{3-/4-}$ at scan rates ranging from 20 to 200 m Vs^{-1} (Fig. 4c). The peak current density of I_{ox} and I_{re} presented a linear increment with the square root of scan rate $v^{1/2}$ (Fig. 4d), indicating that the redox reaction on VS_2 electrodes was diffusion-controlled.[39] The influence of electrolyte pH on the voltammetric response of VS_2 electrodes was examined using the DPV curves with the pH ranging from 5 to 9, as shown in Fig. 4e. With an increase in the electrolyte pH, the peak potential shifted negatively, indicating that the redox reaction on the electrode is determined by a proton transfer process.[40] The oxidation of the amine group in SMX proceeded *via* a pH-dependent reaction.[41] The maximum peak current was achieved at pH = 6 and was selected as the optimal pH. According to the results presented in Fig. 4f, the linear relationship of potential E_{pc} *versus* pH was fitted as E_{pc} (V) = 1.108 − 0.032 pH (R^2 = 0.990). The obtained slope value is smaller than the Nernstian value (59 mV pH^{-1}), demonstrating the same number of protons and electrons involved in the redox reaction.[42]

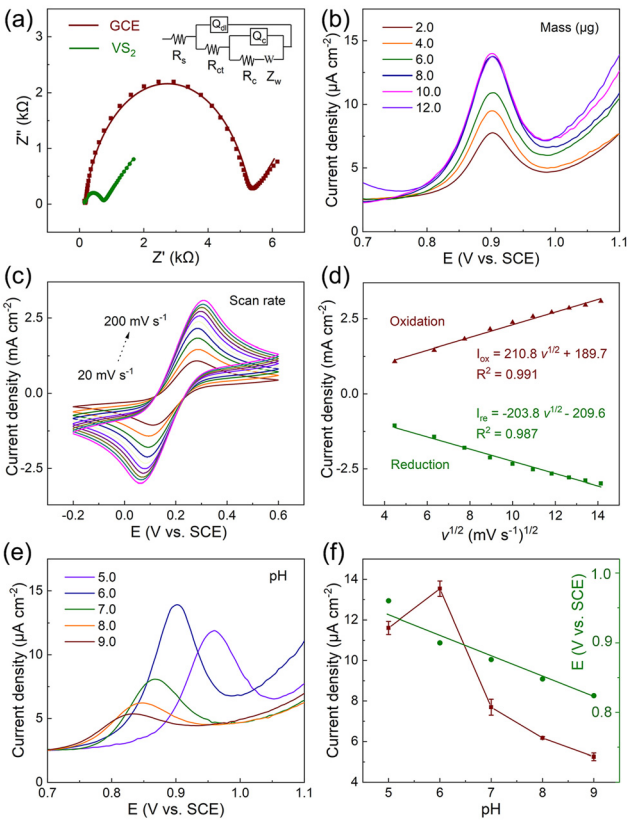

Fig. 4 (a) Impedance plots GCE and VS_2 electrodes in 10 mM $[Fe(CN)_6]^{3-/4-}$. (b) DPV tests of VS_2 electrodes modified with various masses of VS_2 in 10 μM SMX. (c) CV tests of VS_2 electrodes in 10 mM $[Fe(CN)_6]^{3-/4-}$ with various scan rates. (d) Diagrams of I_{ox}/I_{re} *vs.* $v^{1/2}$. (e) DPV curves of 10 μM SMX on VS_2 electrodes with varying pH. (f) Diagrams of I_{pc} and E_{pc} *vs.* pH.

Electrochemical determination of SMX using the VS_2 electrode and its sensing mechanism

The DPV method was employed for the quantitative electrochemical detection of SMX on the VS_2 electrodes, as depicted in Fig. 5a and Fig. S2.† The peak current values on VS_2 electrodes exhibited an upward trend as the SMX concentration increased. A calibration curve for SMX on the VS_2 electrodes was acquired within the linear range of 0.06–10 μM, as illustrated in Fig. 5b. The calibration equation is I_{pc} (μA cm^{-2}) = 1.10c(SMX) (μM) + 2.850 (R^2 = 0.995). Based on the equation, the LOD for SMX on VS_2 electrodes is determined to be 0.047 μM (S/N = 3). DPV tests were performed for the SMX detection on three individual electrodes. Compared to other electrodes used for SMX detection, as presented in Table 1, our SMX electrode achieved a comparatively low LOD for SMX detection and has prospects for application in a wider range for SMX detection.

The sensing mechanism model of VS_2 electrodes is proposed to better illustrate the reason why VS_2 electrodes can be a good candidate for the electrochemical platform towards the sensitive detection of SMX, as presented in Fig. 5c. The voltammetric technique was applied for the determination of SMX on VS_2 electrodes in river water samples. During the electrochemical oxidation of SMX on the VS_2 electrode interface, two electrons and protons are involved in the reaction process. Herein, on behalf of carbon-based nanomaterials with good electrical conductivity, CNTs and rGO were used to compare their charge transfer ability with VS_2. DPV curves of VS_2, graphene and CNT electrodes with 10 μM SMX are presented in Fig. 5d, demonstrating the superior catalytic response of VS_2 toward SMX. Based on the fitting of Nyquist curves of CNTs,

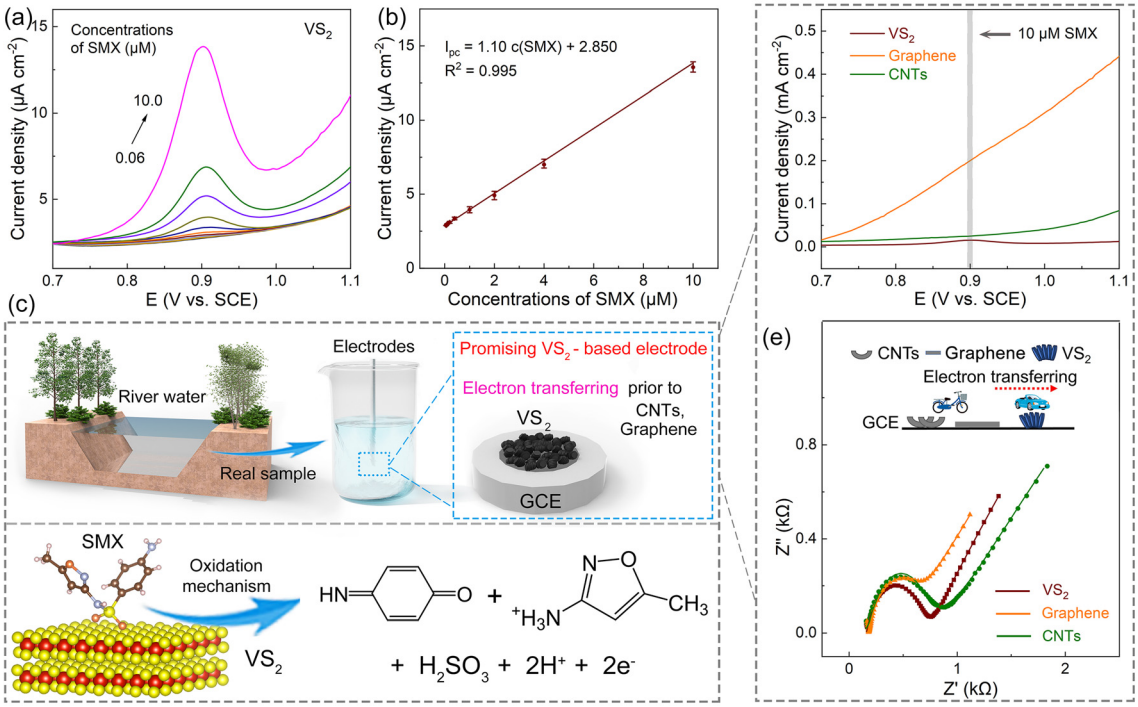

Fig. 5 (a) DPV tests of VS_2 electrodes with SMX concentrations ranging from 0.0 to 10.0 μM. (b) Calibration curve of SMX detection. (c) The proposed detection mechanism of VS_2-based electrodes for sensitive SMX detection. (d) DPV curves of VS_2, graphene and CNTs electrodes with 10 μM SMX. (e) Impedance plots of VS_2, graphene and CNTs electrodes in 10 mM $[Fe(CN)_6]^{3-/4}$.

Table 1 Comparison of detection performance on various electrodes toward SMX

Electrode material	Techniques	Linear range (μM)	LOD (μM)	Ref.
CNTs	DPV	50–10 000	10.0	43
CNTs/PPy	DPV	1.99–10.9	0.413	44
CNTs/*N*,*N*-dimethylfomamide	Amperometry	0.50–110	0.094	5
CNTs/Ti-3	DPV	0.2–100	0.060	45
CNTs/Prussian blue nanocubes	DPV	1.0–10.0	0.038	46
Graphene	DPV	1.0–10.0	0.090	47
Graphene/ZnO	DPV	1.0–220	0.400	48
GO/ITO	DPV	0.1–50	0.060	41
GO/NiO	CV	0.08–550	0.040	49
GO/ZnO	DPV	0.1–1.5	0.029	50
VS_2	DPV	0.06–10	0.047	This work

rGO and VS_2 electrodes presented in Fig. 5e, the VS_2 electrodes showed the lowest R_{ct} values. These results demonstrated the charge transfer ability of VS_2 to be more than those of CNTs and rGO at the electrode interface, validating the prospect of VS_2 as a promising base material for modifying electrodes for sensitive SMX detection. The result is also consistent with the results presented in Table 1. Furthermore, CNT or rGO based nanocomposite modified electrodes presented good detection performance towards SMX as presented in Table 1, supporting the great potential of VS_2 based nanocomposite modified electrodes for the sensitive detection of SMX in the future.

Repeatability, anti-interference, and real sample analysis

To evaluate the reproducibility of VS_2 electrodes for SMX detection (10 μM), DPV tests were conducted on 10 different electrodes in the potential range of 0.7–1.1 V. The DPV curves remained stable at a potential of 0.90 V approximately and maintained good overlapping of the current density, as shown in Fig. 6a. The relative standard deviation (RSD) of the peak current was approximately 2.6%, demonstrating the good repeatability of VS_2 electrodes. Interference experiments were performed using the DPV curves(Fig. 6b), where 10 μM of TMP was used as a typical interfering substance within a concentration range of 0.1–10 μM. Notably, to achieve a continuous synergistic effect of antibacterial activity, the combination of TMP and SMX was usually utilized in the clinical treatment.[51] The interference of TMP in SMX detection in real samples is necessary.

The result demonstrated that TMP did not affect the SMX detection, supporting the potential practical applicability of VS_2 electrodes. Besides, the *i*–*t* technique was performed on VS_2 electrodes in electrolyte containing 10 μM SMX and other interfering substances such as 50 μM CPL, 50 μM FRZ, 50 μM ERY, 50 μM Glu, 100 μM $Na^{\pm}$, 100 μM $K^{\pm}$, 100 μM $Mg^{2\pm}$, and 100 μM $Ca^{2\pm}$, as shown in Fig. 6c and Fig. S3.† The results revealed the exceptional resistance of VS_2 electrodes to interference from other molecules during electrochemical detection.

To validate the detection accuracy of VS_2 electrodes by the DPV method, HPLC was employed to detect SMX in the same real samples.

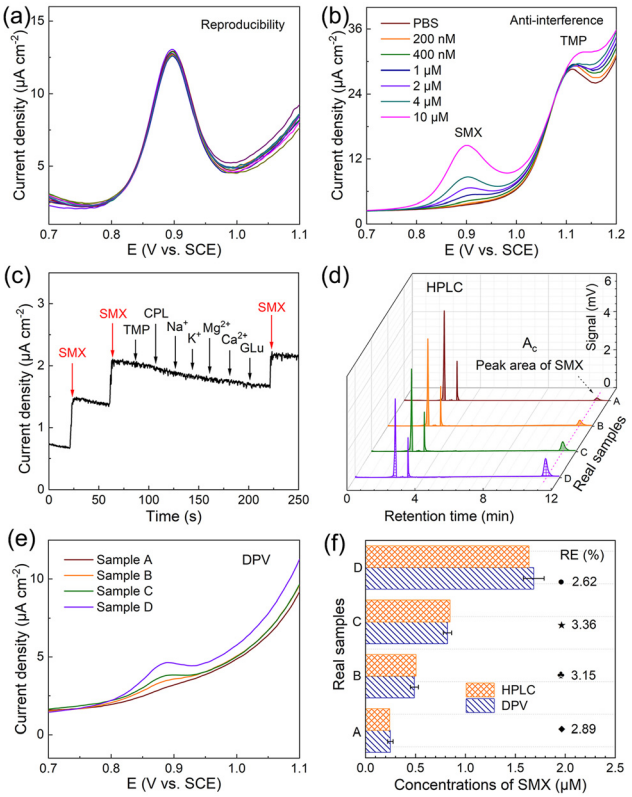

Fig. 6 (a) The reproducibility and (b and c) anti-interference of VS_2 electrodes. (d) HPLC tests for SMX determination in tap samples. (e) DPV responses of VS_2 electrodes. (f) Results comparison within HPLC and DPV tests.

The relative error (RE) is used as the evaluation index calculated using the equation RE = $|(a - b)/b| \times 100\%$, where a and b represent the average values of DPV and HPLC, respectively (μM). Real water samples were prepared by adding a certain mass of SMX to tap water, designated as sample A, B, C, and D. HPLC results were obtained by the computation of the calibration equation, which was determined as $A_c = 8.58 \times 10^3\ C - 206$ ($R^2 = 0.999$). Herein, C is the concentration of SMX (μM), and A_c denotes the peak area at a retention time of 11.3 minutes (μV s), as presented in Fig. 6d. The DPV curves of VS_2 electrodes were constructed for the same real samples, as shown in Fig. 6e. Based on the data comparison of the two methods presented in Fig. 6f, the REs for samples A, B, C and D were determined as 2.89%, 3.15%, 3.36%, and 2.62%, respectively, validating the good accuracy of our electrodes. To further demonstrate the practical applicability of VS_2 electrodes, the recovery performance in river water samples was determined using the standard addition method.[52] As shown in Table S3,† the prepared SMX sensor exhibited good recovery rates (97.4–106.8%) and low RSD values (1.16–1.79%), demonstrating its significant capability for real sample analysis.

Conclusions

This study constructed a sensitive SMX sensor based on layered structured VS_2 nanosheets prepared by the PVP-induced shape control of a hydrothermal synthesis method. Compared to the bare GCE, the VS_2 electrode exhibited higher sensitivity towards SMX oxidation, demonstrating excellent SMX detection performance within a detection range of 0.06–10 μM and a LOD as low as 0.047 μM. The good recovery rates (97.4–106.8%) and practicality of SMX detection in natural waters were validated using the VS_2 electrode. Furthermore, the interference resistance of the VS_2/GCE electrode was examined by adding other potential interfering substances. In conclusion, this research provides a promising approach for the development of electrochemical sensors based on VS_2 composite materials.

Author contributions

Mingjiao Shi: data curation, methodology, formal analysis, and writing – original draft. Peizheng Shi: software, investigation, and data curation. Xinxin Yang: methodology, data curation, and supervision. Ningbin Zhao: investigation and data curation. Mengfan Wu: software and data curation. Jing Li: investigation and data curation. Chen Ye: data curation and methodology. He Li: methodology, supervision, and data curation. Nan Jiang: methodology, supervision, writing – review and editing. Xiufen Li: methodology, data curation, writing – review and editing. Guosong Lai: resources, validation, and software. Wan-Feng Xie: data curation, supervision, writing – review and editing. Li Fu: methodology, supervision, and data curation. Gang Wang: visualization, methodology, and supervision. Yangguang Zhu: methodology, data curation, writing – review and editing. Hsu-Sheng Tsai: visualization, supervision, writing – review and editing. Cheng-Te Lin: conceptualization, writing – review and editing, and funding acquisition.

Conflicts of interest

There are no conflicts to declare.

Acknowledgements

The authors are grateful for the financial support from the National Natural Science Foundation of China (52272053, 52075527 and 52102055), the National Key R&D Program of China (2022YFA1203100, 2022YFB3706602 and 2021YFB3701801), the Ningbo Key Scientific and Technological Project (2021Z120, 2021Z115, 2022Z084 and 2022Z191), the Yongjiang Talent Introduction Program of Ningbo (2021A-037-C and 2021A-108-G), the Youth Fund of Chinese Academy of Sciences (JCPYJ-22030), the China Postdoctoral Science Foundation (2020M681965 and 2022M713243), the CAS Youth Innovation Promotion

Association (2020301), Science and Technology Major Project of Ningbo (2021ZDYF020196 and 2021ZDYF020198), the Project of Chinese Academy of Science (XDA22020602 and ZDKYYQ2020001), and the Ningbo 3315 Innovation Team (2019A-18-C).

References

1 P. S. Kumar, G. Padmalaya, N. Elavarasan and B. Sreeja, *Chemosphere*, 2023, **332**, 138814.
2 P. Balasubramanian, R. Settu, S.-M. Chen and T.-W. Chen, *Microchim. Acta*, 2018, **185**, 396.
3 A. Lamaoui, A. Karrat and A. Amine, *Sens. Actuators, B*, 2022, **368**, 132122.
4 M. Ramya, P. S. Kumar, G. Rangasamy, V. U. Shankar, G. Rajesh and K. Nirmala, *Environ. Res.*, 2023, **216**, 114463.
5 B.-S. He and W.-B. Chen, *J. Braz. Chem. Soc.*, 2016, **27**, 2216–2225.
6 E. Karageorgou, N. Manousi, V. Samanidou, A. Kabir and K. G. Furton, *Food Chem.*, 2016, **196**, 428–436.
7 N. Sun, S. Wu, H. Chen, D. Zheng, J. Xu and Y. Ye, *Microchim. Acta*, 2012, **179**, 33–40.
8 A. L. Krall, S. M. Elliott, M. L. Erickson and B. A. Adams, *Environ. Pollut.*, 2018, **234**, 420–428.
9 H. Sun, H. Qi and H. Li, *Food Anal. Methods*, 2013, **6**, 1049–1055.
10 L. Liu, Q. Wan, X. Xu, S. Duan and C. Yang, *Food Chem.*, 2017, **219**, 7–12.
11 Y. Wang, G. Zhu, D. Wang, M. Huang, J. Yang and J. Liu, *Electrochim. Acta*, 2022, **436**, 141434.
12 R. Chokkareddy, S. Kanchi and G. G. Redhi, *J. Mol. Liq.*, 2022, **359**, 119232.
13 G. Fiori, F. Bonaccorso, G. Iannaccone, T. Palacios, D. Neumaier, A. Seabaugh, S. K. Banerjee and L. Colombo, *Nat. Nanotechnol.*, 2014, **9**, 768–779.
14 P. He, M. Yan, G. Zhang, R. Sun, L. Chen, Q. An and L. Mai, *Adv. Energy Mater.*, 2017, **7**, 1601920.
15 J. Li, Y. Zhang, M. Huo, S.-H. Ho and H.-S. Tsai, *Mater. Today Chem.*, 2022, **26**, 101241.
16 R. Karthik, J. V. Kumar, S.-M. Chen, P. Sundaresan, B. Mutharani, Y. C. Chen and V. Muthuraj, *Ultrason. Sonochem.*, 2018, **48**, 473–481.
17 A. Sharma, P. Mane, B. Chakraborty and C. S. Rout, *ACS Appl. Energy Mater.*, 2021, **4**, 14198–14209.
18 J. Zhou, L. Wang, M. Yang, J. Wu, F. Chen, W. Huang, N. Han, H. Ye, F. Zhao and Y. Li, *Adv. Mater.*, 2017, **29**, 1702061.
19 Z. Shi, H. Huang, C. Wang, M. Huo, S.-H. Ho and H.-S. Tsai, *Chem. Eng. J.*, 2022, **447**, 137469.
20 J. Zhang, C. Zhang, Z. Wang, J. Zhu, Z. Wen, X. Zhao, X. Zhang, J. Xu and Z. Lu, *Small*, 2018, **14**, 1703098.
21 R. Sun, Q. Wei, J. Sheng, C. Shi, Q. An, S. Liu and L. Mai, *Nano Energy*, 2017, **35**, 396–404.
22 J. Kang, F. Xu, C. Zhang, F. Li, O. A. Al-Hartomy, A. Al-Ghamdi, S. Wageh, G. Zhao, T. Yang and H. Zhang, *Adv. Electron. Mater.*, 2022, **8**, 2100567.
23 J. Feng, L. Peng, C. Wu, X. Sun, S. Hu, C. Lin, J. Dai, J. Yang and Y. Xie, *Adv. Mater.*, 2012, **24**, 1969–1974.
24 M. Mulazzi, A. Chainani, N. Katayama, R. Eguchi, M. Matsunami, H. Ohashi, Y. Senba, M. Nohara, M. Uchida and H. Takagi, *Phys. Rev. B: Condens. Matter Mater. Phys.*, 2010, **82**, 075130.
25 A. E. Vilian, S.-K. Hwang, M. J. Lee, B. Park, Y. S. Huh and Y.-K. Han, *Chem. Eng. J.*, 2022, **439**, 135782.
26 A. Sarkar, A. B. Ghosh, N. Saha, G. R. Bhadu and B. Adhikary, *ACS Appl. Nano Mater.*, 2018, **1**, 1339–1347.
27 Y. Zhao, D. Yang, T. He, J. Li, L. Wei, D. Wang, Y. Wang, X. Wang, G. Chen and Y. Wei, *Chem. Eng. J.*, 2021, **421**, 129715.
28 V. M. Varsha and G. Nageswaran, *J. Electrochem. Soc.*, 2020, **167**, 136502.
29 X. Xue, R. Chen, C. Yan, P. Zhao, Y. Hu, W. Kong, H. Lin, L. Wang and Z. Jin, *Adv. Energy Mater.*, 2019, **9**, 1900145.
30 H. Liang, H. Shi, D. Zhang, F. Ming, R. Wang, J. Zhuo and Z. Wang, *Chem. Mater.*, 2016, **28**, 5587–5591.
31 X. Liu, H.-L. Shuai and K.-J. Huang, *Anal. Methods*, 2015, **7**, 8277–8284.
32 S. Sugai, K. Murase, S. Uchida and S. Tanaka, *Solid State Commun.*, 1981, **40**, 399–401.
33 W. G. McMullan and J. C. Irwin, *Solid State Commun.*, 1983, **45**, 557–560.
34 X. Chia, A. Ambrosi, P. Lazar, Z. Sofer and M. Pumera, *J. Mater. Chem. A*, 2016, **4**, 14241–14253.
35 N. Alov, D. Kutsko, I. Spirovová and Z. Bastl, *Surf. Sci.*, 2006, **600**, 1628–1631.
36 Y.-J. Tang, Y. Wang, X.-L. Wang, S.-L. Li, W. Huang, L.-Z. Dong, C.-H. Liu, Y.-F. Li and Y.-Q. Lan, *Adv. Energy Mater.*, 2016, **6**, 1600116.
37 Y. Xue, Z. Zuo, Y. Li, H. Liu and Y. Li, *Small*, 2017, **13**, 1700936.
38 Y. Zhu, X. Li, M. Wu, M. Shi, Q. Tian, L. Fu, H.-S. Tsai, W.-F. Xie, G. Lai, G. Wang, N. Jiang, C. Ye and C.-T. Lin, *Anal. Chim. Acta*, 2023, **1275**, 341607.
39 Y. Zhu, Q. Tian, X. Li, L. Wu, A. Yu, G. Lai, L. Fu, Q. Wei, D. Dai and N. Jiang, *Biosensors*, 2021, **11**, 462.
40 C. Chen, Y.-C. Chen, Y.-T. Hong, T.-W. Lee and J.-F. Huang, *Chem. Eng. J.*, 2018, **352**, 188–197.
41 S.-H. Yeh, M.-S. Huang and C.-H. Huang, *J. Taiwan Inst. Chem. Eng.*, 2022, **131**, 104155.
42 Y. Zhu, X. Li, Y. Xu, L. Wu, A. Yu, G. Lai, Q. Wei, H. Chi, N. Jiang and L. Fu, *Sensors*, 2021, **21**, 1220.
43 S. Issac and K. G. Kumar, *Drug Test. Anal.*, 2009, **1**, 350–354.
44 A. Turco, S. Corvaglia, P. P. Pompa and C. Malitesta, *J. Colloid Interface Sci.*, 2021, **599**, 676–685.
45 L. V. de Souza, O. Tkachenko, B. N. Cardoso, T. M. Pizzolato, S. L. Dias, M. A. Vasconcellos, L. T. Arenas, T. M. Costa, C. C. Moro and E. V. Benvenutti, *Microporous Mesoporous Mater.*, 2019, **287**, 203–210.

46 L. F. Sgobbi, C. A. Razzino and S. A. S. Machado, *Electrochim. Acta*, 2016, **191**, 1010–1017.
47 T. S. Martins, J. L. Bott-Neto, O. N. Oliveira Jr. and S. A. S. Machado, *J. Electroanal. Chem.*, 2021, **882**, 114985.
48 X. Yue, Z. Li and S. Zhao, *Microchem. J.*, 2020, **159**, 105440.
49 M. Shabani-Nooshabadi and M. Roostaee, *J. Mol. Liq.*, 2016, **220**, 329–333.
50 P. S. Kumar, B. Sreeja, K. K. Kumar and G. Padmalaya, *Chemosphere*, 2022, **302**, 134926.
51 L. Ren, M. Chen, J. Zheng, Z. Li, C. Tian, Q. Wang and Z. Wang, *Bioresour. Technol.*, 2021, **338**, 125527.
52 Q. Tian, Y. She, Y. Zhu, D. Dai, M. Shi, W. Chu, T. Cai, H.-S. Tsai, H. Li and N. Jiang, *Sensors*, 2023, **23**, 2870.